

# Proceedings of the Institution of Mechanical Engineers, Part D: Journal of Automobile Engineering

<http://pid.sagepub.com/>

---

## **Numerical studies on the mixing characteristics of exhaust gas recirculation gases with air, and their dependence on system geometries in four-cylinder engine applications**

J N Kim, H Y Kim, S S Yoon, J H Sohn and C R Kim

*Proceedings of the Institution of Mechanical Engineers, Part D: Journal of Automobile Engineering* 2009 223: 585

DOI: 10.1243/09544070JAUTO1040

The online version of this article can be found at:

<http://pid.sagepub.com/content/223/4/585>

---

Published by:



<http://www.sagepublications.com>

On behalf of:



[Institution of Mechanical Engineers](http://www.imechE.org)

---

**Additional services and information for *Proceedings of the Institution of Mechanical Engineers, Part D: Journal of Automobile Engineering* can be found at:**

**Email Alerts:** <http://pid.sagepub.com/cgi/alerts>

**Subscriptions:** <http://pid.sagepub.com/subscriptions>

**Reprints:** <http://www.sagepub.com/journalsReprints.nav>

**Permissions:** <http://www.sagepub.com/journalsPermissions.nav>

**Citations:** <http://pid.sagepub.com/content/223/4/585.refs.html>

>> [Version of Record](#) - Apr 1, 2009

[What is This?](#)

# Numerical studies on the mixing characteristics of exhaust gas recirculation gases with air, and their dependence on system geometries in four-cylinder engine applications

J N Kim<sup>1</sup>, H Y Kim<sup>1\*</sup>, S S Yoon<sup>1</sup>, J H Sohn<sup>2</sup>, and C R Kim<sup>2</sup>

<sup>1</sup>Department of Mechanical Engineering, Korea University, Seoul, Republic of Korea

<sup>2</sup>Research & Development Center, Hyundai-Kia Motor Company, Gyeonggi-Do, Republic of Korea

*The manuscript was received on 15 October 2008 and was accepted after revision for publication on 5 January 2009.*

DOI: 10.1243/09544070JAUTO1040

**Abstract:** To achieve low nitrogen oxide (NO<sub>x</sub>) emissions and combustion reliability, the variation in the geometry of the exhaust gas recirculation (EGR) system should be optimized. However, the layout process essentially fixes the position of a conventional EGR system, and modifying the intake manifold geometry tends to be economically unjustifiable for a commercial engine. In the present study, two types of EGR system, namely 'linked single' and 'individual' EGR systems, are proposed and their performances are evaluated numerically. Parametric studies were performed using a three-dimensional numerical model to assess the mixing uniformity of the intake air and EGR gases. The distribution of the mixed gases into the four runners, which force the mixed gases into the four combustion cylinders, is predicted. Three different geometries of the EGR system are considered: single, side-feed individual, and top-feed individual configurations. These geometries reflect the means by which the EGR gases are supplied into the four cylinders. These three configurations are called cases A, B, and C respectively, and their corresponding detailed geometries are identified as A1 to A9, B1 to B17, and C1 to C10, which give a total of 36 computational runs. It was found that case A5 with a hole angle of 60° yielded the most optimal operating mixing and distribution condition. In general, the single systems were found to be superior to the individual systems, among which the top-feed system tended to be slightly more advantageous for mixing than the side-feed individual system owing to the symmetric supply of the top-feed system. The flow of the throttle-valve system, which controls the mass flowrate of the intake air, was used as the validation case; Hyundai-Kia Motor Co. provided the experimental data, which were compared with the computational results.

**Keywords:** exhaust gas recirculation, exhaust gas recirculation distribution, mixing characteristics, linked single exhaust gas recirculation, individual exhaust gas recirculation

## 1 INTRODUCTION

The development of advanced-engine control systems for the modern four-stroke gasoline engine is being driven by the demand for higher fuel economy and increasingly stringent exhaust emissions standards. Additionally, emissions compliance must be

maintained to increase service duration while on-board-diagnostics (OBD-II) requirements are satisfied. These requirements for lower emissions and enhanced combustion reliability pose a great technical challenge to automobile engineers.

Exhaust gas recirculation (EGR) has recently been recognized as an attractive method for reducing nitrogen oxide (NO<sub>x</sub>) emissions by recycling of the high-temperature exhaust gases. Within the EGR system, pumping is enhanced by increased intake manifold pressure, and the system heat loss can be

\*Corresponding author: Department of Mechanical Engineering, Korea University, 1, 5-Ga, Anam-dong, Sungbuk-gu, Seoul, 136-701, Republic of Korea. email: kimhy@korea.ac.kr

minimized by recycling the hot exhaust gases. The performance of the current EGR technique can be improved by feeding uniformly mixed and equally distributed EGR gases into the multi-cylinder engine; for non-uniformity limits the degree to which  $\text{NO}_x$  emission can be lowered and, generally, has a negative influence on the engine cycle and fuel consumption rate [1–5].

For a single system, EGR gases are fed into the intake manifold of the air stream from the side; see Fig. 1(a) for the ‘conventional’ system. Often, the EGR gases are fed through three linked holes with an additional passage that improves the mixing between the EGR gases and air; see Fig. 1(b) for the ‘linked’ system. Next these mixed gases pass through the surge tank shown in Fig. 2 and then finally are distributed into four runners. Changing the position of the EGR inlet and the intake manifold geometry can improve the mixing quality, prior to the feeding of the gases into the combustion cylinders. Optimization of these geometrical changes may further reduce  $\text{NO}_x$  emissions and improve combustion stability. From a practical point of view, however, modifying the geometry of the intake manifold seems to be economically unviable for commercial engines. Also, changing the position of

the EGR inlet is often limited by the layout of the other engine parts [6–9].

In the present study, the performance of two different EGR systems, called ‘linked single’ and ‘individual’ EGR systems, are investigated numerically. This work compares the characteristics of the mixing and distribution of the EGR gases and the intake air that are fed into the runners and cylinders. All numerical simulations are performed by using a commercial code STAR-CD [10], based on a fully three-dimensional Reynolds Averaged Navier–Stokes (RANS) formulation, which employs a standard  $k-\epsilon$  turbulence closure model.

For validation of our numerical results, a complex flow of gases in the pipe of the throttle-valve system, which controls the mass flowrate of the intake air, is simulated, and its results are compared against the experimental data provided by Hyundai-Kia Motor Co.

## 2 NEW EGR SYSTEMS: LINKED SINGLE AND INDIVIDUAL

Figures 1(a) and (b) show the schematic diagrams of the conventional and linked EGR systems respectively.

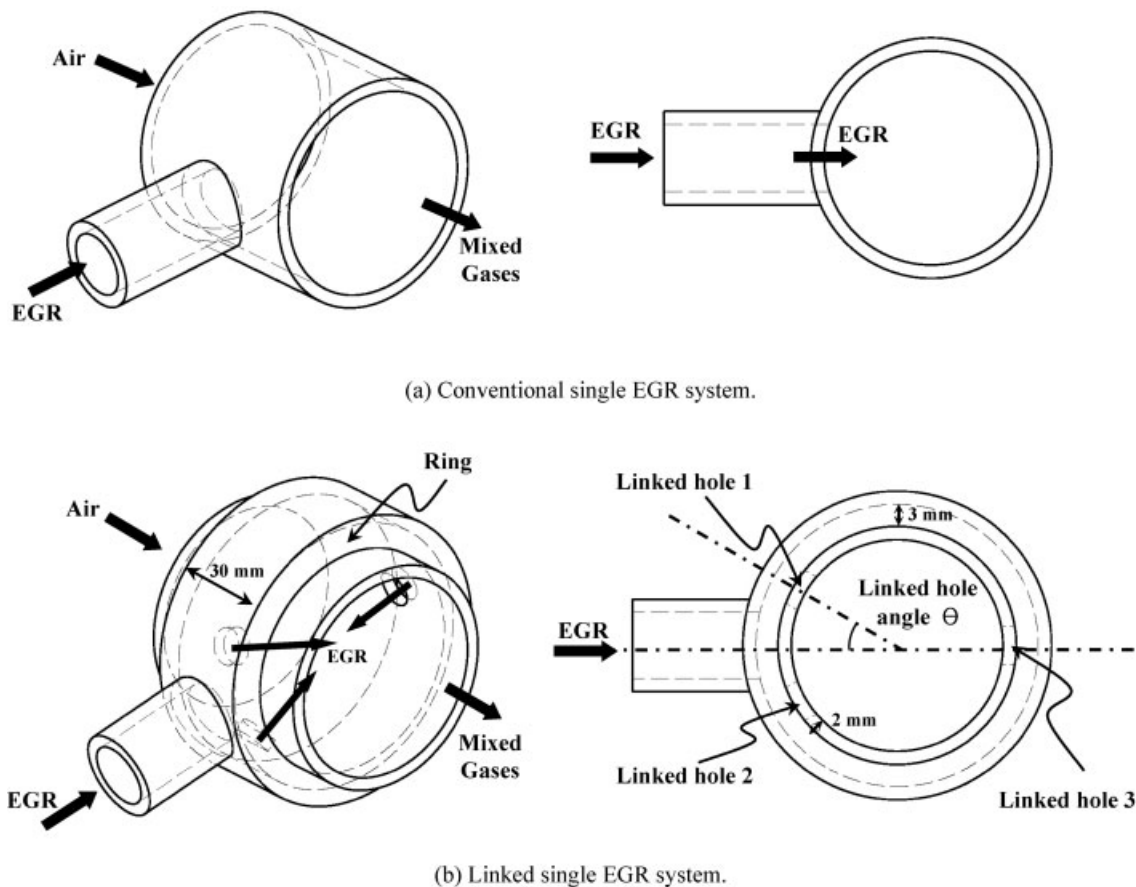


Fig. 1 Schematic diagrams of conventional and linked single EGR supply systems

In the conventional EGR system, EGR gases are supplied into the intake manifold. The EGR inlet is installed at a location downstream of the throttle valve: this is the benchmark case A1. On the other hand, the linked single system employs an additional ring with three holes that envelop the intake pipe, into which the EGR gases are supplied. The ring's outer diameter is 3 mm larger than that of the intake pipe diameter, and the ring's width is 30 mm. As shown in Fig. 1(b), holes 1 and 2 are separated at a sector angle of  $2\theta$ . Half the sector angle, defined as the 'linked hole angle', is changed from  $30^\circ$  to  $90^\circ$  by an increment of  $10^\circ$ , whose computational runs correspond to cases A2 to A8. Hole 3 is situated exactly opposite to or  $180^\circ$  apart from the EGR inlet. All three holes are equally sized (2 mm diameter) and the sum of their areas is the same as the area of the EGR inlet; as a result, the velocities at the inlet and the holes are the same. Similar to the conventional case A1, the EGR inlet is located 45 mm downstream from the throttle valve.

The term 'individual' is given for the systems shown in Figs 2(c) and (d) because the EGR gases are fed separately and directly into each runner without passing the EGR gases through the surge tank, whereas the 'single' EGR systems employ a feeding pipe that connects to the surge tank (see Figs 2(a) and (b)). Figures 2(c) and (d) represent the side-feed and top-feed EGR systems respectively, consisting of both main and branch pipes. For the computational runs of cases B1 to B17 and C1 to C10, both the length and the diameter of the branch pipe are varied to identify the best possible configuration of the system.

### 3 MODELLING DESCRIPTIONS

#### 3.1 Governing equations

The conservation equations for continuous gas phase can be described by the following equation, with the variables given in Table 1

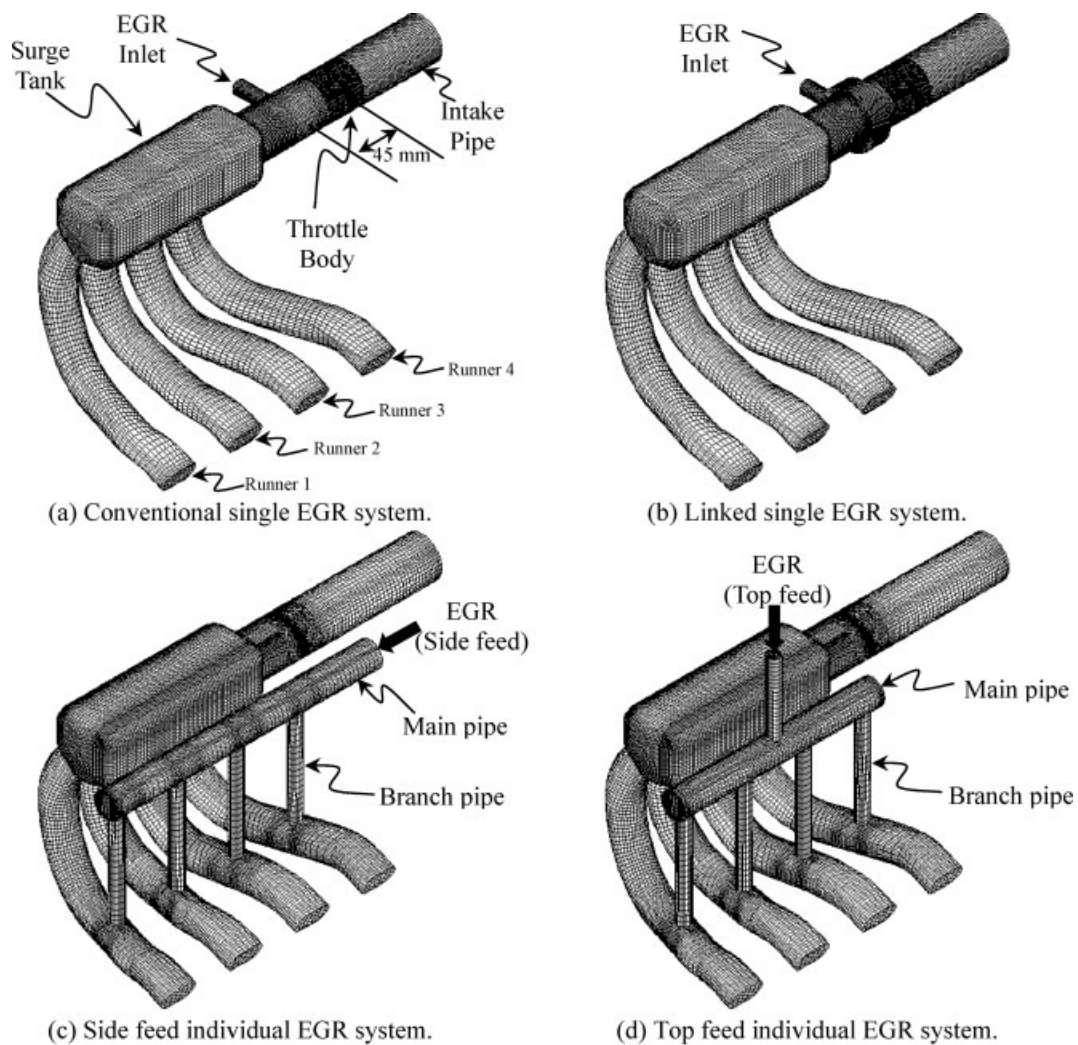


Fig. 2 Generated grids for various EGR supply systems

**Table 1** Generalized equations

Equation	$\varphi$	$\Gamma_\varphi$	$S_\varphi$
Continuity	1	0	0
Momentum	$u_i$	$\mu_e$	$-\frac{\partial p}{\partial x_i} + \frac{\partial}{\partial x_j} \left[ \mu_e \frac{\partial u_j}{\partial x_i} - \frac{2}{3} \left( \rho k + \mu_t \frac{\partial u_k}{\partial x_k} \right) \delta_{ij} \right]$
Turbulent kinetic energy	$k$	$\mu + \frac{\mu_t}{\sigma_k}$	$G_k - \rho \varepsilon$
Dissipation rate	$\varepsilon$	$\mu + \frac{\mu_t}{\sigma_\varepsilon}$	$\frac{\varepsilon}{k} (c_1 G_k - c_2 \rho \varepsilon)$
Species	$Y_s$	$\frac{\dot{\lambda}}{C_p} + \frac{\mu_t}{\sigma_Y}$	0
Energy	$h$	$\frac{\dot{\lambda}}{C_p} + \frac{\mu_t}{\sigma_h}$	0

$\mu_e = \mu + \mu_t$  (effective viscosity).  $G_k = \mu_t \left( \frac{\partial u_i}{\partial x_j} + \frac{\partial u_j}{\partial x_i} \right) \frac{\partial u_i}{\partial x_j}$  (turbulent generation).

$$\frac{\partial}{\partial t} (\rho \varphi) + \frac{\partial}{\partial x_j} (\rho u_j \varphi) = \frac{\partial}{\partial x_j} \left( \Gamma_\varphi \frac{\partial \varphi}{\partial x_j} \right) + S_\varphi \quad (1)$$

### 3.2 Geometry and mesh generation

The engine system considered herein has four cylinders, each with a volume of 1495 cm<sup>3</sup>, a bore size of 75.5 mm, and a stroke of 83.5 mm. A conventional *butterfly* valve is used to control the throttle device. As shown in Fig. 1(a), the inner diameter of the intake pipe is 48 mm, within which a sealing valve or throttle valve is installed at a tilted angle of 17°, as shown in Fig. 3. The sealing angle of the throttle valve is 10°, which allows the flow passage of 7° only for the scenarios considered herein. The commercial programs CATIA and ICEM CFD [11] are used to generate the meshes for the entire computational domain. The mesh for all components is designed as a hexahedral type, except for the intake pipe because of its complex crescent shape (not shown in Fig. 1), for which a tetrahedral mesh is used. A typical calculation requires a total of 380 000 nodes.

### 3.3 Numerical procedures

Simulation is initiated with a quasi-steady state solution, obtained from a previous run, to achieve rapid convergence. Numerical stability is generally guaranteed with the application of the Courant–Friedrichs–Lewy condition. Typically, the time step  $\Delta t = 1^\circ$  crank angle is used for the given operating conditions of 2000 r/min and 2 bar (break mean effective pressure). A fully implicit scheme is used for the time-marching calculation to secure numerical stability. To solve the flow field, the pressure implicit with splitting of operators (PISO) algorithm is coupled with the upwinding scheme [12]. The standard RANS  $k$ – $\varepsilon$  model is used to model turbulence.

As for boundary conditions, the inlet air pressure is set to the standard atmospheric pressure of 1 bar and the corresponding velocities are extrapolated. The ratio of the mass flowrate of air to that of EGR gases is approximately  $\dot{m}_a / \dot{m}_{\text{EGR}} = 7.3$ , or sometimes it is defined as the EGR rate, as  $\dot{m}_{\text{EGR}} / (\dot{m}_{\text{EGR}} + \dot{m}_a) = 0.12$ . In theory, during the intake stroke of expansion, a low pressure develops inside the cylinder

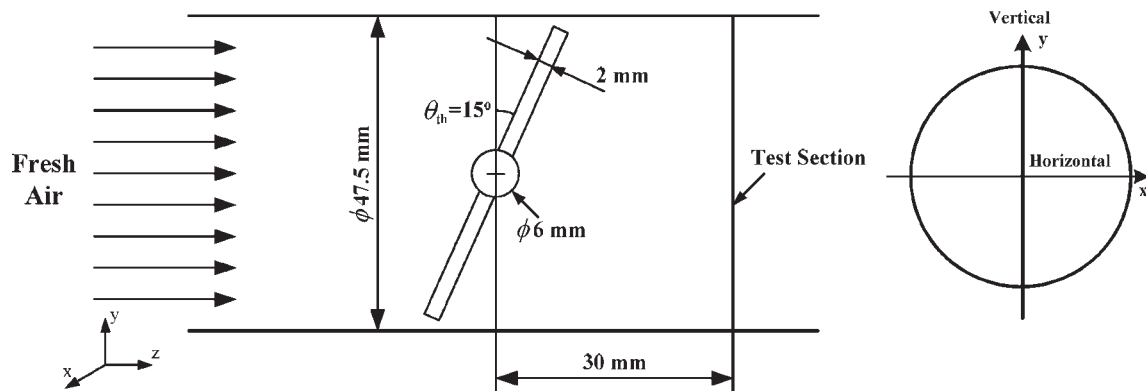


**Fig. 3** Schematic diagrams of the throttle body for validation

which, in turn, induces acceleration of the local gas flow. Here the pressure variation can be modelled as a sinusoidal graph, and the pattern of the corresponding velocity is assumed to be exactly the opposite of the pressure variation [13], a fact which is also supported by the experimental data from Hyundai-Kia Motor Co. This theoretically assumed velocity is used as a specified boundary condition.

## 4 RESULTS AND DISCUSSION

### 4.1 Validation

The flow inside the throttle body, shown in Fig. 2, is simulated and validated against the experimental data from Hyundai-Kia Motor Co. The dimension of the throttle body used for validation is shown in Fig. 3. The inner diameter of the throttle body is 47.5 mm and its throttle angle is  $\theta_{\text{throttle}} = 15^\circ$  while its sealing angle is  $\theta_{\text{throttle}} = 0^\circ$ . The ratio of the mass flowrate of air to EGR gases is approximately  $\dot{m}_a/\dot{m}_{\text{EGR}} = 9.0$  or an EGR rate of 0.1. The experiment is based on a hot-wire anemometer technique that provides data on the air axial velocity passing through the throttle valve [14–18]. From both model and experiment, the velocity data of the flow at the 30 mm downstream location from the valve centre for quasi-steady state are obtained, as indicated in Fig. 3. Figure 4 compares the air axial velocities from the experiment and model; a nearly symmetric velocity distribution is shown in the horizontal direction while the velocity distribution in the vertical direction is highly asymmetric owing to the tilted angle of the throttle valve. Further comparison of the pressure data from experiment and the modelling indicates an agreement in the maximum pressure drop across the

throttle valve, which reaches approximately 55 kPa, and this agreement confirms the reliability of the modelling results.

### 4.2 Flow characteristics behind the throttle valve

An accelerated flow exists behind the throttle valve with a small throttle angle  $\Delta\theta_{\text{throttle}} = 7^\circ$  because of the small slit passage; this is the case when the engine is under light operation, known as part load, in which 90 per cent of the pressure is lost across the throttle valve. This severe change in flow pressure characteristics across the valve has substantial influence over the flow downstream and subsequent air mixing with the EGR gases [19–21].

As shown in Fig. 5, the airflow passing through the upper slit is highly accelerated, exceeding a flow speed of 300 m/s; the bottom slit also accelerates flow because of its small flow passage. The flow in the upper slit remains in the upper region while the flow in the bottom region tends to rise toward the upper region. To confirm this flow pattern, the cross-sectional view of line A–A from Fig. 5 is shown in Fig. 6. Here two distinct flow motions are shown: a vortical motion, later causing helical or spiral flow motion downstream, exists in the upper region while the bottom flow rapidly rises toward the upper vortical region. These motions reverse the direction of the downstream flow, which in turn results in a longer residence time for the EGR gases and more homogeneous mixing between the EGR gases with the incoming air.

Figure 7(a) shows the reversed flow on the  $x$ – $z$  plane while the vertical and rising motions formed behind the throttle valve are shown on the  $x$ – $y$  plane as in Fig. 7(b), in which the contour variable is the

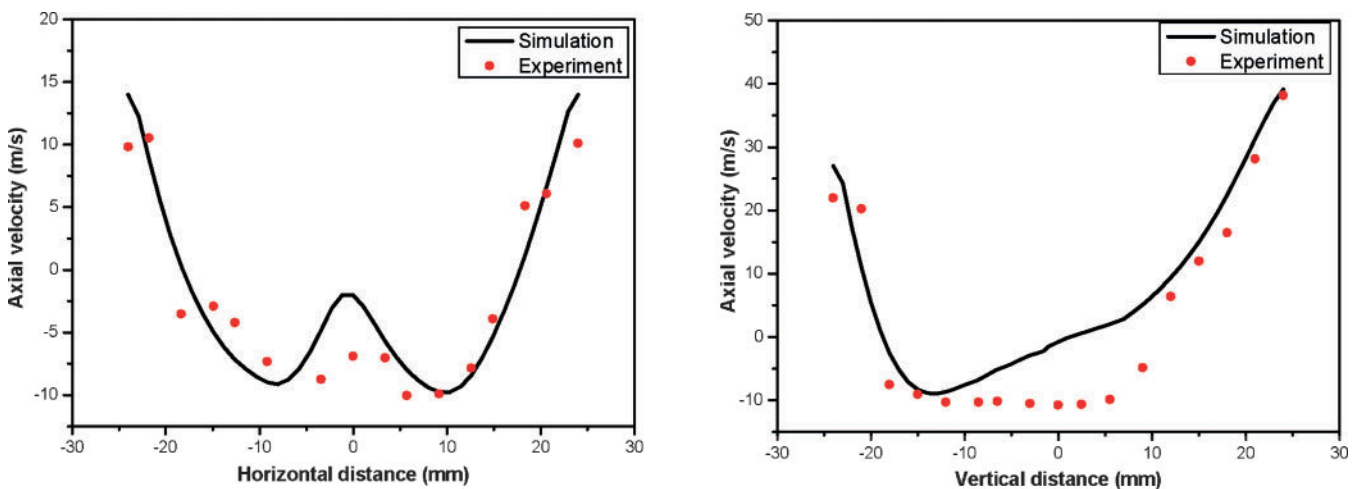


Fig. 4 Comparison with experimental data for validation

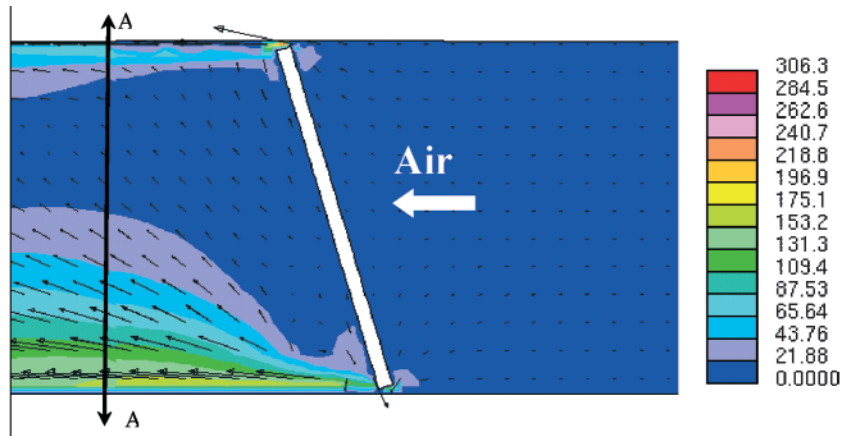


Fig. 5 Flow field at the cross-section of the throttle valve

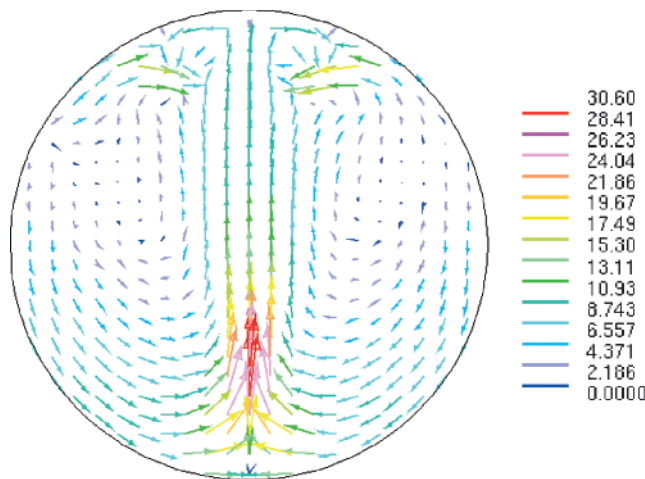


Fig. 6  $u$  and  $v$  velocity components of the flow field after the throttle valve

axial velocity in the  $z$  direction. As shown in Fig. 7(b), the upper and lower regions are the areas where the flow acceleration is prominent, whereas the right and left regions are clearly the reversed flow

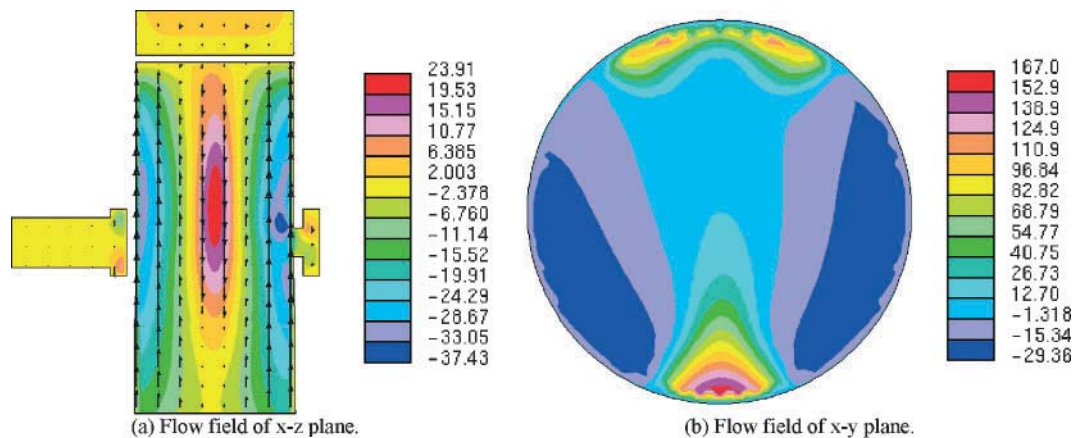


Fig. 7  $w$  velocity component of the flow field after the throttle valve

region with an indication of negative velocities. Most EGR gases are first drawn into the throttle valve in reversed flow. These mixed gases pass through the surge tank and then finally are fed into the four cylinders.

Figure 8 represents the streamlines of the mixed gases when each engine or cylinder is in full operation. Normally, firing or engine operation proceeds, starting from cylinder 1, followed by cylinders 3, 4, and 2. When cylinder 1 is opened, the gases are fed into cylinder 1, and a similar pattern of feeding applies when cylinders 3, 4, and 2 are opened. Simply because of geometrical reasons, the largest and the smallest amount of gases are fed into cylinders 1 and 4 respectively; compare the streamlines shown in Figs 8(a) and (c).

### 4.3 Linked single EGR system

In the linked single EGR system, the three holes provide homogeneous mixing between the EGR gases and air, which in turn provides uniform dis-

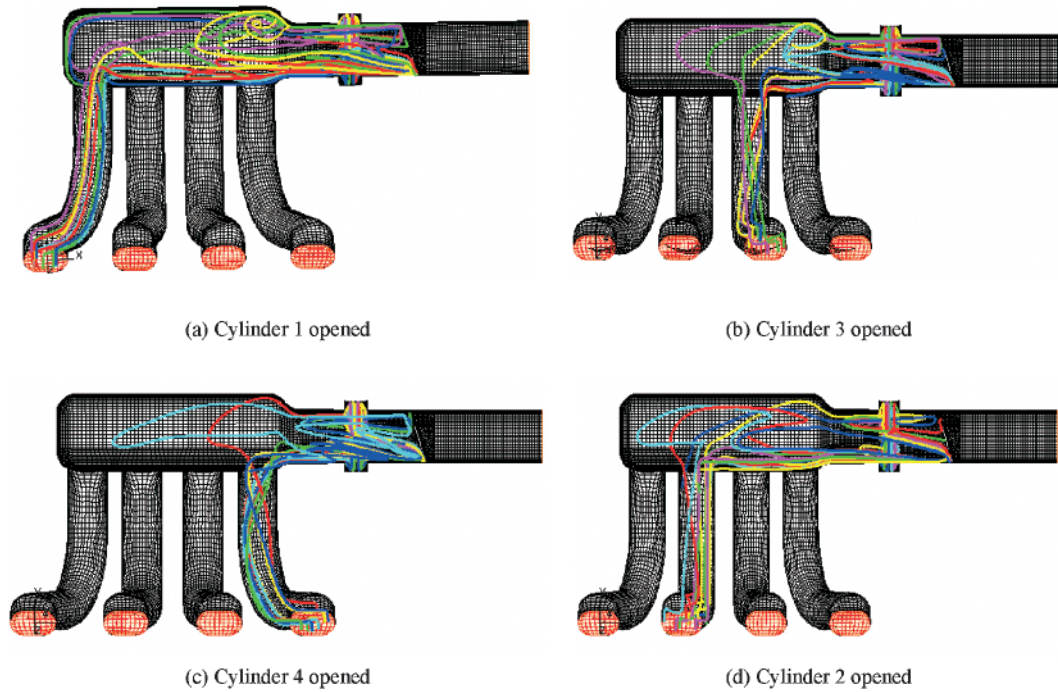


Fig. 8 Path line of the EGR stream when each intake valve is fully opened (firing order)

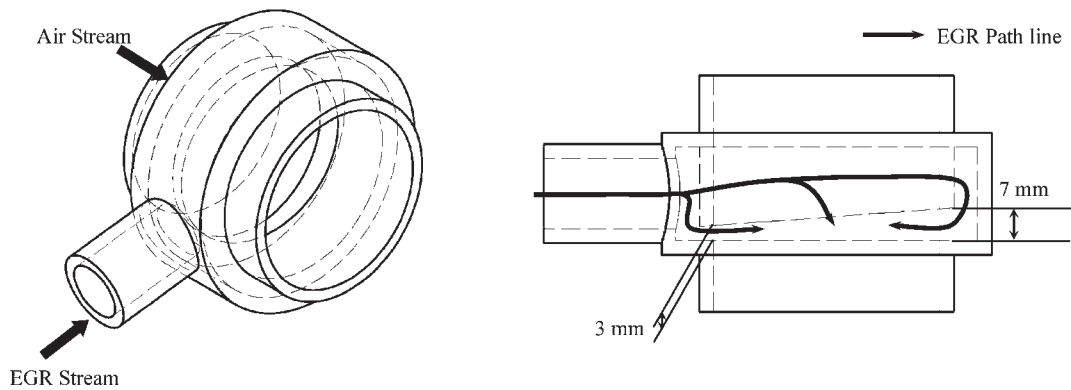


Fig. 9 Schematic diagrams of the slit-type single EGR system (case A9)

tribution into the four cylinders [22]. A cylindrically shaped ring is installed at the cross point between the intake pipe and the EGR inlet, as shown in

Fig. 1(b). The linked hole angle  $\theta$  shown in Fig. 1(b) is varied from  $30^\circ$  to  $90^\circ$  at an increment of  $10^\circ$ , yielding a total number of seven cases, which are

Table 2 Mixture distribution rates and EGR maldistribution rates for a linked single EGR system

Case	Linked hole angle (deg)	Mixture distribution rate (%)				EGR maldistribution rate (%)			
		Cylinder 1	Cylinder 2	Cylinder 3	Cylinder 4	Cylinder 1	Cylinder 2	Cylinder 3	Cylinder 4
Only air	NA	26.75	24.51	24.82	23.92	NA	NA	NA	NA
Case A1	NA	30.44	23.96	24.73	20.87	13.43	11.76	11.96	10.63
Case A2	30	30.23	23.97	24.85	21.14	13.35	11.77	12.01	10.76
Case A3	40	30.15	23.67	24.89	21.23	13.32	11.64	12.03	10.80
Case A4	50	30.12	23.44	24.93	21.52	13.31	11.54	12.05	10.93
Case A5	60	29.77	23.25	25.15	21.83	13.18	11.45	12.14	11.07
Case A6	70	29.63	23.78	25.20	21.38	13.12	11.68	12.16	10.86
Case A7	80	29.64	24.13	25.24	20.98	13.13	11.84	12.18	10.68
Case A8	90	29.80	23.74	25.48	20.98	13.19	11.67	12.28	10.68
Case A9	NA	29.95	23.54	25.24	21.62	13.25	11.58	12.18	10.97

NA, not applicable.

referred to as cases A2 to A8. Note that case A1 represents the conventional or benchmark configuration shown in Fig. 1(a). Furthermore, instead of having holes, the inner part of the ring is cut with a slit angle, creating a passage for mixing of the EGR

gases with air (Fig. 9); this scenario is referred to as case A9. These aforementioned cases are summarized in Table 2.

In an ideal system, a perfectly uniform distribution would provide 25 per cent of the mixed gases into each cylinder, since there are four. However, in reality, runner 1 (see Fig. 2(a)) always receives the largest amount of the mixed gases (see also Table 2), a trend which indicates that the largest gas amount goes to runner 1. Runners 2 and 3 receive roughly comparable amounts of the mixed gases and cylinder 4 receives the least. Figure 8 shows the flow as streamlines when each cylinder is open in the order of cylinder 1, followed by cylinders 3, 4, and 2. When cylinder 1 is opened, the mixed gases are injected towards the left end of the surge tank and finally fed into runner 1. On the other hand, when cylinder 4 is opened, some mixed gases travel the entire surge tank (see Fig. 8(c)) and then are fed into runner 4, whose flow pattern tends to reduce the EGR gas supply into runner 4.

An EGR rate of 0.12 is used for all parametric studies, except for the validation case. Thus, in theory, all four runners and cylinders should receive the same 0.12 portion of the EGR rate if the EGR

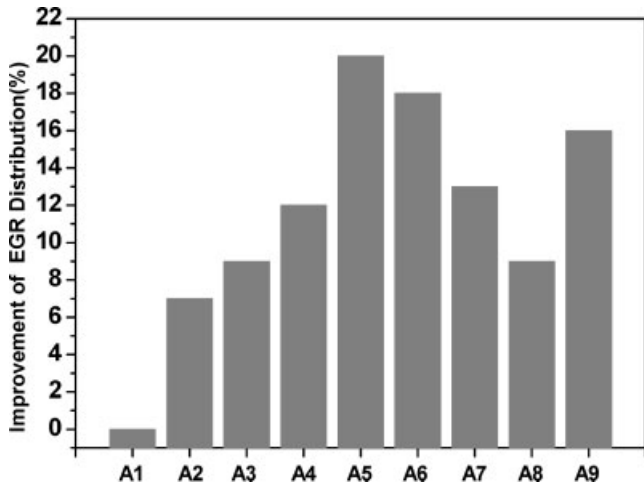


Fig. 10 Improvement in the EGR distribution for various linked single EGR systems based on standard deviation

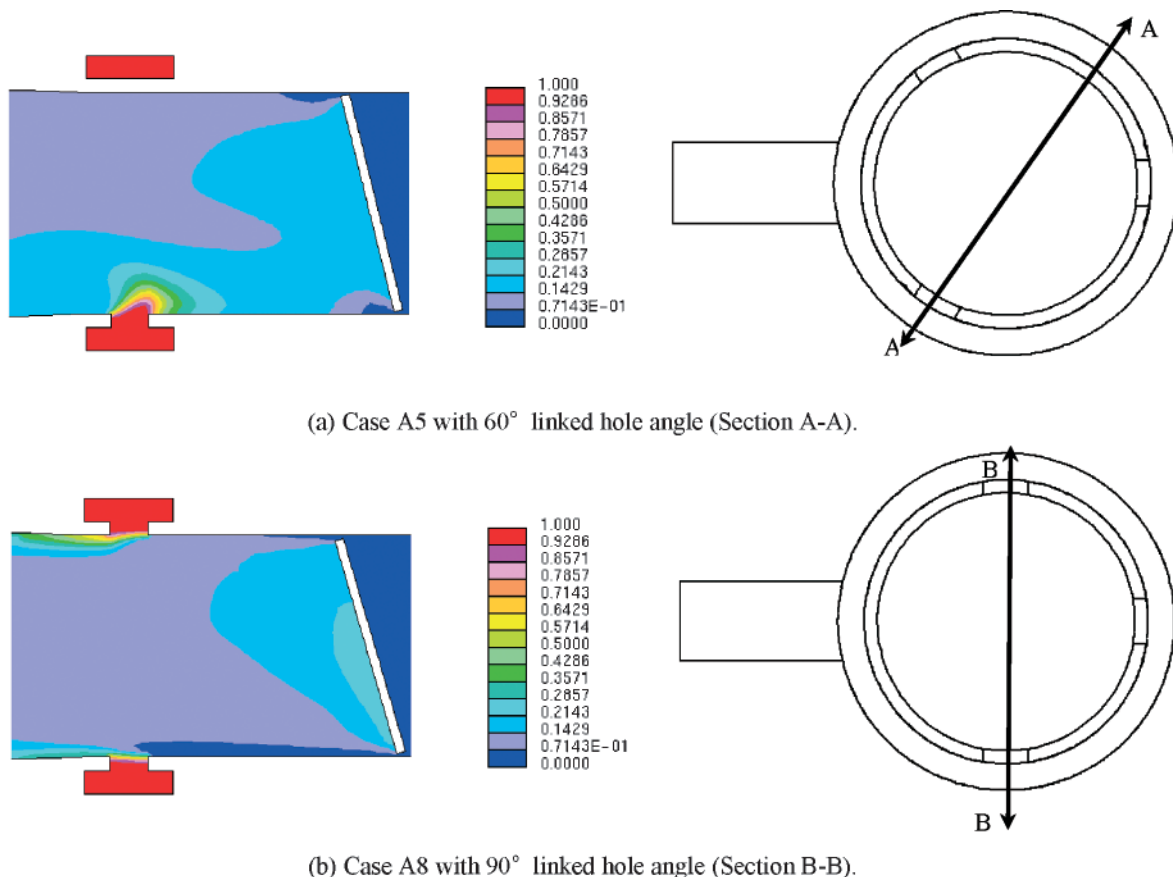


Fig. 11 EGR mass fraction at each cross-section including the linked hole

gases are ‘perfectly’ and ‘uniformly’ mixed with incoming air. However, the simulation results from Table 2, which indicate that the EGR rate decreases from cylinder 1 to cylinder 4, is related to the fact that the mixed gases travel a relatively longer path.

The percentage difference of the EGR rate is computed with respect to the value of 0.12 (or 12 per cent) for each cylinder. Then the standard deviation is computed, which is again normalized by the benchmark value of case A1. The normalized

standard deviation from Fig. 10 shows that case A5 yields the smallest deviation (or largest improvement). The trend indicates that there is an optimum linked angle at 60° and that mixing performance deteriorates when increasing and decreasing the linked angle from 60°. It is noteworthy that the slit-type system of case A9 seems to yield favourable mixing conditions because its relative improvement is comparable with those of cases A5 and A6. Overall, the linked single EGR systems generally yield an

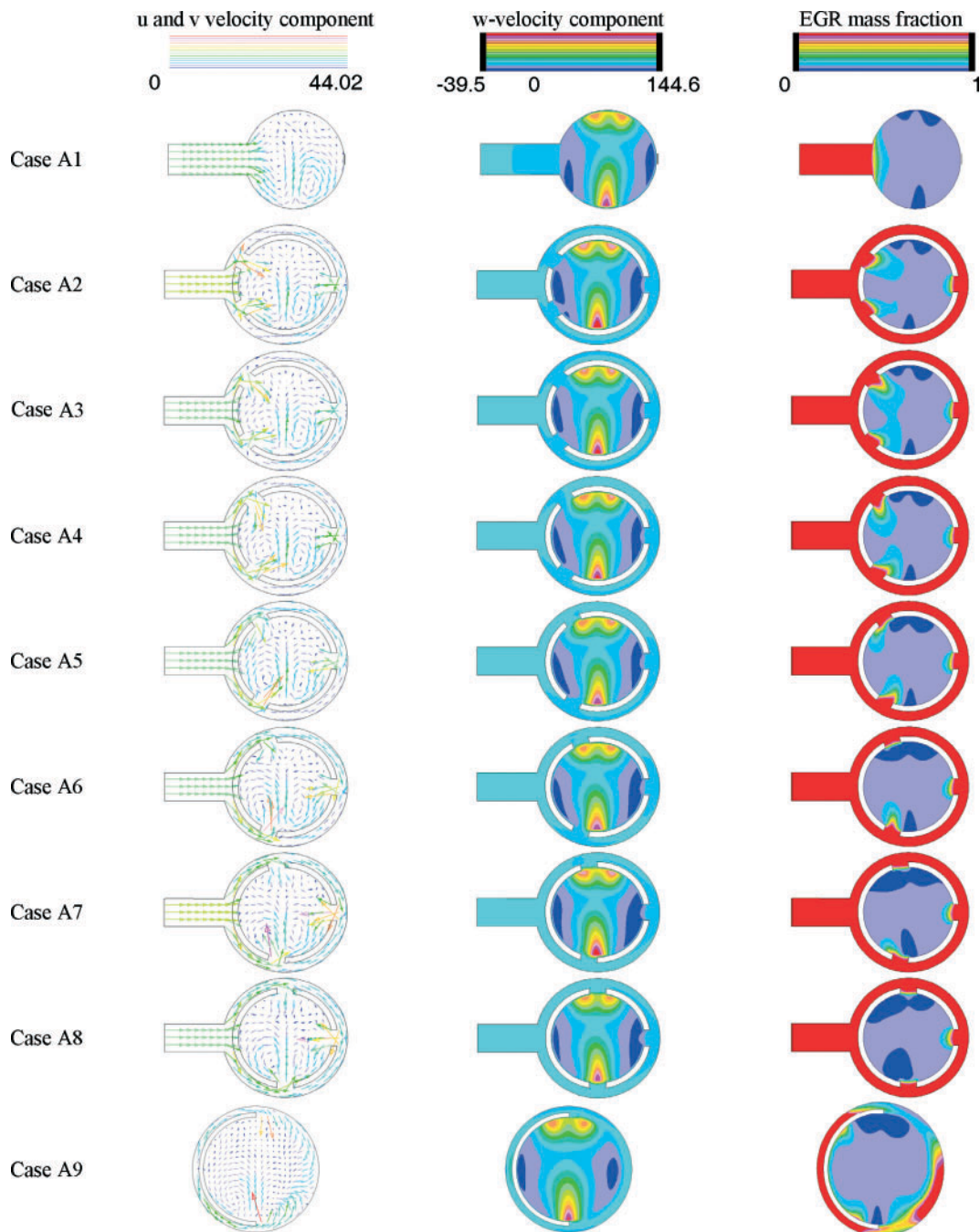


Fig. 12 Flow field and EGR mass fraction at the cross-section of the linked single EGR system

improved mixing condition over the conventional or benchmark case A1.

Figures 11(a) and (b) show the snapshots of the EGR mass fraction of cases A5 and A8 respectively, which are taken at the cross-section of lines A–A and B–B. As mentioned previously, flow accelerates in the upper and bottom regions owing to the small flow passage across the throttle valve with a small throttle angle of  $7^\circ$ . The right and left sides are the reversed-flow regions in which the flow is recirculated behind the throttle valve. The difference between cases A5 and A8 is as follows: the EGR supply holes are located near the reversed flow region in case A5 whereas the holes are located farther away from the reversed flow in case A8. Consequently, case A5 yields a longer residence time for the EGR gases to be mixed while they are recirculated in the reversed flow than for case A8. These flow patterns of the EGR gases through the holes are summarized in Fig. 12. Penetration of the EGR gases into the air stream is optimal in case A5 as the effect of the reversed flow is maximum at the

linked angle of  $60^\circ$ . When the linked angle is  $90^\circ$ , the EGR gases are carried by the high-speed air stream of the upper and lower regions and fed directly into the runners without being well mixed with air, thus yielding a relatively poor performance in mixing and engine operation.

The reversed flow results from the rising and vortical motions induced across the throttle valve. In other words, it exists even if there is no EGR supply from the side injection. Thus any EGR linked system that takes good advantage of this reversed flow would provide a mixing condition in accordance with an engineer's intention.

#### 4.4 Individual EGR system

As previously described, the individual EGR system consists of both main and branch pipes, as shown in Fig. 2(b). Parametric studies for the side-feed and top-feed systems are referred to as cases B1 to B17 and cases C1 to C10, respectively. The distribution of

**Table 3** Mixture distribution rate and EGR maldistribution rate for individual EGR systems

Case	Specification*	Mixture distribution rate (%)				EGR maldistribution rate (%)			
		Cylinder 1	Cylinder 2	Cylinder 3	Cylinder 4	Cylinder 1	Cylinder 2	Cylinder 3	Cylinder 4
Only air	NA	26.75	24.51	24.82	23.92	NA	NA	NA	NA
Case A1	Linked single EGR	30.44	23.96	24.73	20.87	13.43	11.76	11.96	-11.02
Case B1	BD, 15 mm (fixed); BL, 50 mm (varied)	10.47	11.61	25.14	52.87	5.07	6.07	12.14	23.16
Case B2	BD, 15 mm (fixed); BL, 80 mm (varied)	10.71	9.45	25.96	52.88	5.18	4.99	12.48	23.16
Case B3	BD, 15 mm (fixed); BL, 100 mm (varied)	14.23	12.59	25.70	47.48	6.76	6.55	12.37	21.30
Case B4	BD, 15 mm (fixed); AR, 1:2 (varied)	8.03	14.23	26.73	51.01	3.93	7.34	12.81	22.53
Case B5	BD, 15 mm (fixed); AR, 1:4 (varied)	14.23	12.59	25.70	47.48	6.76	6.55	12.37	21.30
Case B6	BD, 15 mm (fixed); AR, 1:6 (varied)	16.93	13.97	22.98	46.12	7.94	7.21	11.21	20.82
Case B7	BD, 10 mm (fixed); BL, 50 mm (varied)	18.65	23.89	24.99	32.47	8.68	11.73	12.07	15.62
Case B8	BD, 10 mm (fixed); BL, 80 mm (varied)	19.80	22.65	24.83	32.72	9.17	11.19	12.00	15.72
Case B9	BD, 10 mm (fixed); BL, 100 mm (varied)	20.31	23.03	24.79	31.87	9.38	11.36	11.99	15.38
Case B10	BD, 10 mm (fixed); upstream	20.22	23.70	26.16	29.92	9.34	11.65	12.57	14.57
Case B11	BD, 10 mm (fixed); convergent	20.45	23.01	24.29	32.25	9.44	11.35	11.77	15.53
Case B12	BD, 10 mm (fixed); opposite	18.50	21.69	25.52	34.29	8.62	10.77	12.30	16.35
Case B13	BD, 10 mm (fixed); below	20.33	22.70	25.98	30.99	9.39	11.21	12.49	15.01
Case B14	BL, 100 mm (fixed); BD1–BD2–BD3–BD4 = 8–8–10–10	15.76	17.64	30.30	36.30	7.44	8.94	14.27	17.15
Case B15	BL, 100 mm (fixed); BD1–BD2–BD3–BD4 = 10–10–8–8	29.18	30.23	18.43	22.15	12.95	14.40	9.19	11.21
Case B16	BL, 100 mm (fixed); BD1–BD2–BD3–BD4 = 10–10–9.5–9.5	22.51	25.09	23.32	29.08	10.29	12.25	11.36	14.22
Case B17	BL, 100 mm (fixed); BD1–BD2–BD3–BD4 = 10–10–9–9	24.23	26.72	21.78	27.28	10.99	12.94	10.69	13.46
Case C1	BD, 15 mm (fixed); BL, 50 mm (varied)	11.67	20.26	24.05	44.02	5.61	10.13	11.67	20.06
Case C2	BD, 15 mm (fixed); BL, 80 mm (varied)	12.23	18.45	22.00	47.32	5.87	9.31	10.78	21.25
Case C3	BD, 15 mm (fixed); BL, 100 mm (varied)	12.06	17.65	21.74	48.55	5.79	8.94	10.67	21.68
Case C4	BD, 15 mm (fixed); AR, 1:2 (varied)	12.44	20.67	18.06	48.33	5.96	10.31	9.03	21.60
Case C5	BD, 15 mm (fixed); AR, 1:4 (varied)	12.06	17.56	21.74	48.55	5.79	8.90	10.67	21.68
Case C6	BD, 15 mm (fixed); AR, 1:6 (varied)	12.46	16.09	22.58	48.87	5.97	8.22	11.04	21.79
Case C7	BD, 10 mm (fixed); BL, 50 mm (varied)	19.47	23.58	23.44	33.51	9.03	11.60	11.41	16.04
Case C8	BD, 10 mm (fixed); BL, 80 mm (varied)	21.08	22.19	22.29	34.44	9.70	10.99	10.91	16.41
Case C9	BD, 10 mm (fixed); BL, 100 mm (varied)	21.41	21.52	22.54	34.53	9.84	10.69	11.02	16.45
Case C10	BD, 10 mm (fixed); upstream	21.91	22.29	23.33	32.47	10.05	11.03	11.36	15.62

\*NA, not applicable; BD, branch diameter; BL, branch length; AR, area ratio of the branch pipe to the main pipe; (fixed), the parameter that is fixed; (varied), the parameter that is varied.

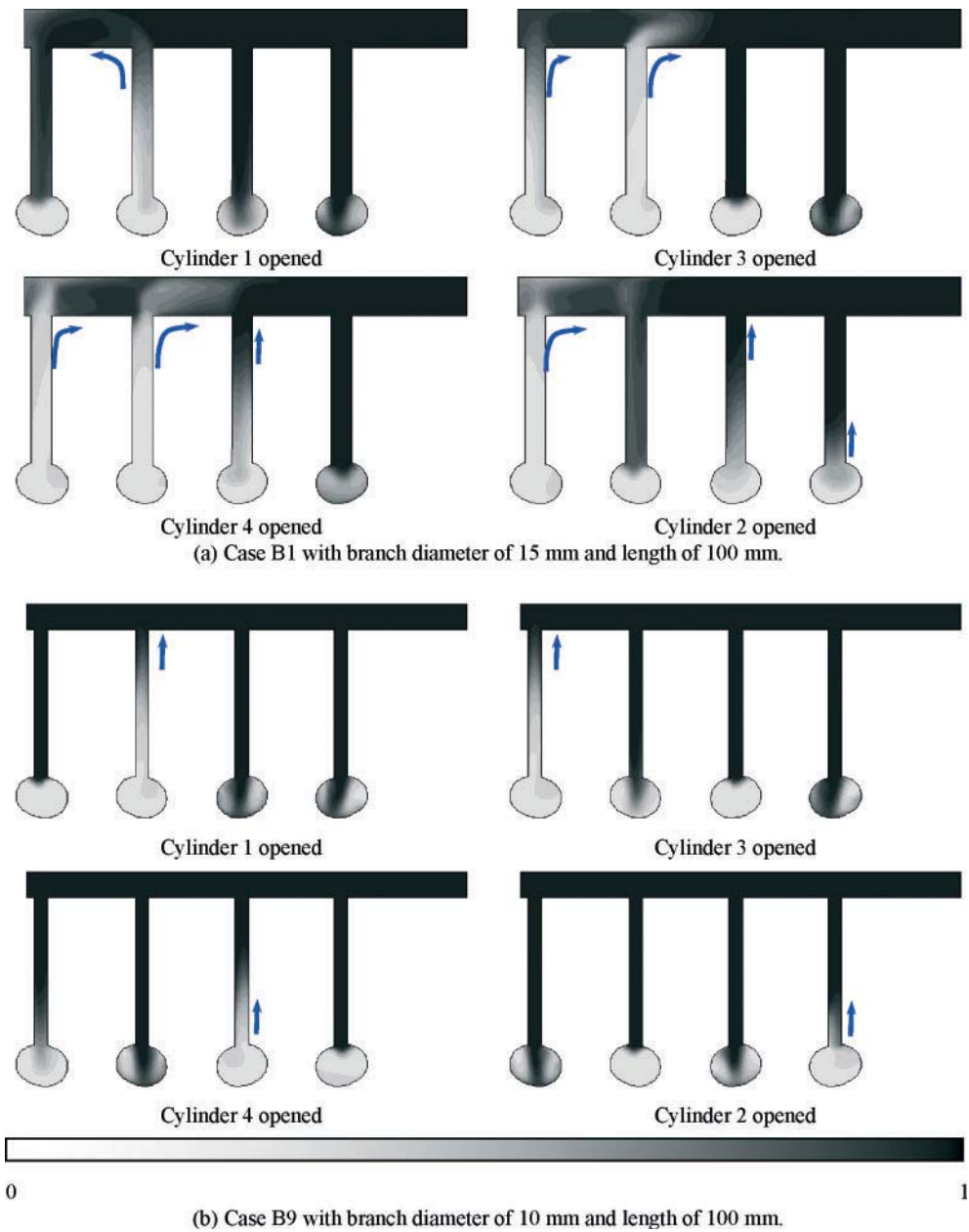


**Fig. 13** EGR mass fraction and ingress of fresh air to the individual EGR system (firing order)

the mixed gases into each cylinder and their EGR rates are summarized in Table 3. From cases B1 to B6, the branch diameter is fixed as 15 mm while the branch length and the area ratio of the branch pipe to main pipe are varied. As for the effect of the branch length, cases B7 to B13 are simulated under the fixed branch diameter value of 10 mm. For cases B14 to B17, the effect of the changing branch diameter (i.e. BD1–BD2–BD3–BD4) on the mixing uniformity is studied. Similar parametric measures are applied to the top-feed systems of cases C1 to C10.

From Table 3, cylinder 4 generally takes in the largest amount of mixed gases and EGR rate; this pattern is always true for all cases in the individual systems, although the magnitudes of their differences slightly differ from one case to another. The EGR gases fed into the branch pipe are shown in Fig. 13(a) at the given branch diameter of 15 mm. As shown, the EGR concentration is the largest at cylinder 4 regardless of which cylinder is opened. When cylinder 1 opens, ‘drawing down’ [21] occurs, by which the flow at the nearest branch is entrained into the firing cylinder. Interestingly, flows from all

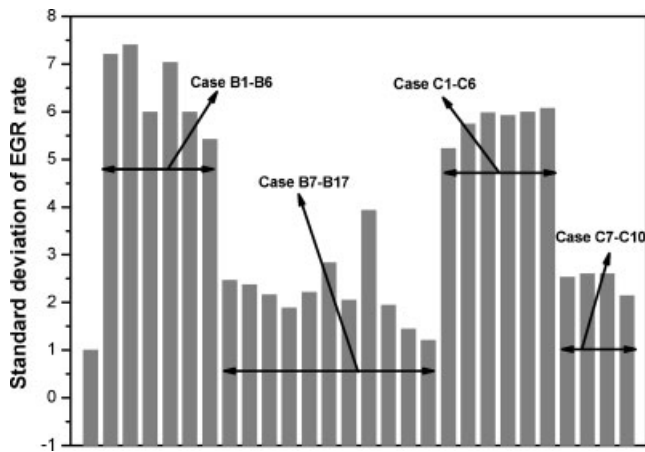


Fig. 14 Standard deviation of the EGR rate to each cylinder for individual EGR systems

first three branches are entrained into the fourth branch in the event of firing of cylinder 4. The 'drawing down' causes a highly asymmetric distribution of the EGR gases into the branches.

When the branch diameter decreases from 15 mm to 10 mm, the EGR feeding into cylinder 4 is reduced. Compare the mixture distribution rates of cases B1 to B6, and B7 to B13; also compare Figs 13(a) and (b). It is noteworthy that the amount of flow into each cylinder increases in the order of cylinders 1, 2, 3, and 4 whose pattern applies to all side-feed cases B1 to B17, except that, in some cases, the percentage amounts into cylinders 1 and 2 are nearly the same.

Figure 14 compares the normalized standard deviation of the EGR rate for cases B1 to B17 and C1 to C10 with respect to that of the benchmark case A1. Generally, cases B7 to B17 of 10 mm branch diameter yields a smaller deviation than cases B1 to B10 of 15 mm branch diameter; thus the smaller branch diameter is recommended to improve mixing. The effect of the area ratio of cases B4 to B6, the install position (i.e. upstream, convergent, opposite, and below) of cases B10 to B13, and altering branch diameter seems to be insignificant. As for the top-feed cases C1 to C10, the favourable effect of the smaller branch diameter also applies, as in the side-feed cases B1 to B17. Cases C7 to C10 of 10 mm branch diameter yields an improved mixing condition over cases C1 to C6 of 15 mm branch diameter.

## 5 CONCLUSIONS

A fully three-dimensional RANS formulation that employs a standard  $k-\epsilon$  turbulence closure model was applied to simulate the mixing of EGR gases

with air. A flow behind the throttle valve was simulated and the simulation results were compared with the experimental data provided by Hyundai-Kia Motor Co. Parametric studies of 36 computational runs provided information that can be used as the benchmark data for optimization of the EGR system.

As for the linked single system, it was found that the hole location (or the linked angle) of the attached ring is important for inducing homogeneous mixing. A reversed flow was formed behind the throttle valve, inducing vortical and rising motions downstream. When the EGR gases were well entrained into the reversed flow, mixing between the EGR gases and the air stream improved. When the hole was located where the rising motion was dominant, it also helped the EGR gases to be entrained into the air stream. However, the effect of the reversed flow seemed to be more dominant than that of the rising flow for better mixing.

As for the individual EGR systems, the top-feed system was slightly better than the side-feed system for mixing because of the symmetry of the top-feed system. None of the individual EGR cases was found to be superior to even the poorest case of the linked single system; thus the linked single system is definitely advantageous and recommended for future EGR designs. A branch diameter of small size is recommended because it minimized the drawing-down behaviour in the event of cylinder firing. The effect of area ratio, install position, and altering branch diameter seemed to be negligible.

## REFERENCES

- 1 Neame, G. R., Gardiner, D. P., Mallory, R. W., and Rao, V. K. Improving the fuel economy of stoichiometrically fuelled S.I. engines by means of EGR and enhanced ignition. SAE paper 952376, 1995.
- 2 Hawley, J. G., Wallace, F. J., Cox, A., Horrocks, R. W., and Bird, G. L. Reduction of steady state NOx levels from an automotive diesel engine using optimised VGT/EGR schedules. SAE paper 1999-01-0835, 1999.
- 3 Baert, R. S. G., Beckman, D. E., and Veen, A. Efficient EGR technology for future HD diesel engine emission targets. SAE paper 1999-01-0837, 1999.
- 4 Yokomura, H., Kohketsu, S., and Mori, K. EGR system in a turbocharged and intercooled HD diesel engine. JSAE paper 20015459, 2001.
- 5 Berry, I. J. and Brunt, M. F. J. Improved control of EGR during speed/load transients. SAE paper 960068, 1996.

- 6 **Siewert, R. M., Krieger, R. B., Huebler, M. S., Baruah, P. C., Khalighi, B., and Wesslau, M.** Modifying an intake manifold to improve cylinder-to-cylinder EGR distribution in a DI diesel engine using combined CFD and engine experiments. SAE paper 2001-01-3685, 2001.
- 7 **Shaw, C. T., Lee, D. J., Richardson, S. H., and Pierson, S.** Modelling the effect of plenum-runner interface geometry on the flow through an inlet system. SAE paper 2000-01-0569, 2000.
- 8 **Ahn, H. S., Cho, K. M., and Choi, J. K.** Analysis of EGR distribution characteristics in intake manifolds and plenum chamber with 1-D and 3-D hybrid calculations. In Proceedings of the 15th Internal Combustion Engine Symposium, Seoul, Republic of Korea, July 1999, pp. 443–448 (Society of Automotive Engineers of Japan, Tokyo).
- 9 **Borghi, M., Mattarelli, E., and Montorsi, L.** Integration of 3D-CFD and engine cycle simulations: application to an intake plenum. SAE paper 2001-01-2512, 2001.
- 10 *STAR-CD methodology and user guide, version 3.15A*, 2001 (CD-adapco, New York).
- 11 *ICEM CFD manual*, 2000 (ANSYS ICEM CFD Engineering, Canonsburg, Pennsylvania).
- 12 **Issa, R. I.** Solution of the implicitly discretised fluid flow equations by operator-splitting. *J. Comput. Phys.*, 1986, **62**, 20–65.
- 13 **Benajes, J., Reyes, E., Galindo, J., and Peidro, J.** Predesign model for intake manifolds in internal combustion engine. SAE paper 970055, 1997.
- 14 **Jorgensen, F. E.** *Directional sensitivity of wire and hot-film probes*, DISA Information Publication 11, 1971, pp. 31–37 (DISA Elektronik, Skovlunde, Denmark).
- 15 **Janjua, S. I., McLaughlin, D. K., Jackson, T., and Lilley, D. G.** Turbulence measurements in a confined jet using a six-orientation hot-wire probe technique. *AIAA J.*, 1984, **22**(4), 514–515.
- 16 **Dvorak, K. and Syred, N.** The statistical analysis of hot-wire anemometer signal in complex flow fields. In Proceedings of the DISA Conference, Leicester, UK, 1972, vol. 2, pp. 4–10 (University of Leicester Press, Leicester).
- 17 **Lee, G. H., Choi, Y. D., and Han, S. H.** Measurement of developing turbulent flow in a U-bend of circular cross-section. *J. Mech. Sci. Technol.*, 2007, **21**(2), 348–359.
- 18 **King, C. F.** *Some studies of vortex devices – vortex amplifier performance behaviour*. PhD Thesis, University College of Wales, Cardiff, Wales, 1978.
- 19 **Chen, J. L. and Chen, G.** Throttle body at engine idle-tolerance effect on flow rate. SAE paper 951057, 1995.
- 20 **Alsemgeest, R., Shaw, C. T., Richardson, S. H., and Pierson, S.** Modelling the time-dependent flow through a throttle valve. SAE paper 2000-01-0659, 2000.
- 21 **Heywood, J. B.** *Internal combustion engine fundamentals*, 2000 (McGraw-Hill, New York).
- 22 **Wang, X., Feng, Z., and Forney, L. J.** Computational simulation of turbulent mixing with mass transfer. *Computers Structs*, 1999, **70**, 447–465.